This is the accepted manuscript made available via CHORUS. The article has been published as:

Microscopic origin of giant piezoelectricity in ferroelectric math xmlns="http://www.w3.org/1998/Math/MathML">mrow>mi>x/mi>msub>mrow>mi>Bi/mi>mo>(/mo>mi>Ni/mi>/mrow>mrow>mn>0.5/mn>/mrow>/msub>msub>mi>Hf/mi>mrow>mn>0.5/mn>/mrow>/msub>mrow>mo>)/mo>/mrow>msub>mi mathvariant="normal">O/mi>mn>3/mn>/msub>/mrow>mo>−/mo>mrow>mrow>mo>(/mo>mn>1/mn>mo>−/mo>mi>x/mi>mo>)/mo>/mrow>msub>mi>PbTiO/mi>mn>3/mn>/msub>/mrow>/math> beyond the morphotropic phase boundary

K. Datta, Naveen Kumar, A. Upadhyay, B. Mihailova, and Rajeev Ranjan

Phys. Rev. B **104**, L140104 — Published 25 October 2021

DOI: 10.1103/PhysRevB.104.L140104

Microscopic Origin of Giant Piezoelectricity in Ferroelectric xBi($Ni_{0.5}Hf_{0.5}$)O_3-(1-x)$PbTiO_3$ beyond Morphotropic Phase Boundary

K. Datta,[1] Naveen Kumar,[2] A. Upadhyay,[2] B. Mihailova,[1] and Rajeev Ranjan[2]

[1] *Department of Earth Sciences, University of Hamburg, Grindelallee 48, Hamburg 20146, Germany.**
[2] *Department of Materials Engineering, Indian Institute of Science, Bangalore 560012, India.*

Local structural correlations in a novel ferroelectric solid solution (xBi($Ni_{0.5}Hf_{0.5}$)O_3-(1-x)$PbTiO_3$ at $x = 0.39$) has been drawn out through atomistic modeling against neutron pair distribution functions and complementary Raman scattering measurements. By examining polar displacements of different cations from the refined structural models, we reveal the distributions of cation-specific dipolar fluctuations at the key composition where the maximum piezoelectric response was recorded. It becomes clear that the unusual structural modifications observed after the poling are simply a manifestation driven by the varying extent of the dipolar fluctuations and not a structural transformation caused by the adaptive cationic displacements. Moreover, in addition to strong dipolar flexibility under electric field, both poled and unpoled ceramics exhibit orientation-independent polarized Raman scattering, which is more typical of a dipolar glass with a responsive and polarizable matrix than a polycrystalline material composed of ferroelectric domains. Therefore, compared to other analogous xBi(Me)O_3-(1-x)$PbTiO_3$ systems, the current material is a unique case where chemical substitution has led to a highly polarizable ionic-covalent matrix that seems to be the key ingredient to generate giant piezoelectricity at a composition beyond the morphotropic phase boundary.

Local structure and dynamics of disordered and chemically complex ferroelectrics are exciting topics because often they affect the properties in an unpredictable way[1,2]. Although structure-property relationships in such materials are in general described well by phenomenological theories[3–5], corresponding physical manifestations remain indistinct in many cases. For example, it is not yet well formulated how the flattening of energy surfaces near a inter-ferroelectric phase transition or a tricritical point can be translated and identified by micro- or nano-structural features beyond the crystallographic description of the average structure. Notably, nearly five decades after the observation of the so called morphotropic phase boundary (MPB) in the famous $Pb(Zr_xTi_{1-x})O_3$ solid solution, a generic theory unifying different analytical concepts and structural models for PZT and in other similar systems is still missing[6–9]. Meanwhile, it has become clear that atomic-level understanding of how chemistry impacts the competing local interactions might be a key to unlock this conundrum[10,11]. Consequently, there is a rapid change in the paradigm of structural studies – focussing exclusively on local structures and dynamics underneath the canonical crystallographic manifestations[1,12,13]. In particular, new nano-scale structural phenomena in perovskite polar oxides have been uncovered[14–17], which are proved to be crucial in developing a broader understanding of the interrelationships among dielectric, electromechanical, and mechanical properties in ferroic materials.

Currently, Pb and Bi containing solid solutions with general formula xBiMeO_3-(1-x)$PbTiO_3$ have become leading materials for many applications due to their stable and superior piezoelectric properties[18–20]. Moreover, these systems offer a path to build better environmentally-friendly materials suitable for a wide range of sensor and actuator applications. In general, PZT-like MPB-behaviour has been identified in this class, where considerable enhancement in piezoelectric response at critical compositions, usually triggered by a structural-instability is found[21,22]. However, the solid solution xBi($Ni_{0.5}Hf_{0.5}$)O_3-(1-x)$PbTiO_3$ (xBNH-PT) has become a major talking point in this field because of its unusual structure-property exhibition with the composition: The maximum piezoelectric response was recorded at a point beyond the distinct MPB region, where the average structure evolved to a seemingly single pseudocubic phase. A detailed structural study using x-ray scattering[23] further revealed that the pseudocubic phase at $x = 0.39$ transforms into a more prominent tetragonal phase on the application of electric field. Consequently, in this case, the common polarization-rotation or polarization-extension concepts[24,25] cannot be applied to justify the nontrivial structure-property curve, rather it proves that the ideas based on the average structure should not be presumed as generic. In this context, we have applied the total neutron scattering and Raman scattering techniques to resolve its atomic-to-mesoscopic scale structural correlations and dynamics to understand better the link between structural changes and properties at the key composition.

In particular, statistical information on cation-specific dipolar disorder developed in the system at the key composition were extracted from the structural models which were refined against the pair distribution function (PDF) at room temperature. In addition to the static picture, the dynamic effects from the dipolar disorder manifested strongly polarized Raman scattering intensity that suggest the dominance of the incipient ferroic distortions beyond the inherent ferroic domains. Based on these results, as well as considering the characteristics of similar xBiMeO_3-(1-x)$PbTiO_3$ solid solutions, it is evident that the xBNH-PT at $x = 0.39$ is a unique material mimicking

the ergodic state of a polar glass, for which electromechanical properties are additionally boosted by the easy polarization dynamics of a responsive matrix.

Ceramic samples of xBNH-PT at $x = 0.39$ were prepared following the solid-state synthesis route[23]. Total neutron scattering experiments at ambient conditions were carried out on the GEM diffractometer[26] at ISIS facility in the U.K. Data correction and subsequent reduction to generate the PDFs were performed using the GUDRUN package. Experimental PDFs were then modelled applying the reverse Monte Carlo (RMC) method as implemented in the RMCProfile software[27]. The starting structural models were $18 \times 18 \times 18$ supercells of the tetragonal unit cells derived from the Rietveld refinements of the powder diffraction data. Each model consisted of 29160 atoms, and we applied nearest-neighbor distance-window constraints together with a weak bond-valence sum restraint in the iterations to ensure the refined models remain chemically valid. To produce good statistics of the structural parameters, we performed 50 independent RMC runs for poled and unpoled ceramics, and each run was continued for approximately 10^7 accepted moves. The analyses of the refined structural models were done using the DISCUS package[28]. Some additional details and plots of the data are given in the supplementary information[29].

Analytically the PDF is defined as the probability of finding atom-pairs separated by a distance r in real space. So PDFs virtually provide a nano-scale view within a system through weighted histograms of all atom-atom distances[30,31]. Hence, atomistic modelling against PDFs helps to extract nano-to-mesoscopic level structural details in a quantitative manner[32,33]. Given that the structure and properties of ferroelectric materials are predominantly driven by their inherent polar distortions, we have followed the idea developed in the geometric phase approach[34] to examine the local dipolar features (magnitude and direction) stemming from different types of cations. To this end, polar displacement vectors ($\delta\vec{r}$) were derived from the refined models as follows:

$$\delta\vec{r}_{\mathrm{Pb/Bi}} = \vec{r}_{\mathrm{Pb/Bi}} - \frac{1}{12}\sum_i \vec{r}_{iO}$$
$$\delta\vec{r}_{\mathrm{Ti/Ni/Hf}} = \vec{r}_{\mathrm{Ti/Ni/Hf}} - \frac{1}{6}\sum_i \vec{r}_{iO} \qquad (1)$$

For the evaluation of these parameters, the directions of those vectors ($\delta\widehat{r}$) were mapped onto cubic stereograms as shown in Fig.1, which manifest an excellent overview of the cation-specific local polarization correlation function within the system, and how it evolved after the electric field treatment. Clearly, the cations exhibit significant dispersion in their shift-directions, yet maintaining a statistical preference along $[001]_{pc}$. In other words, the stereographs depict the development of high degeneracy of the local ferroic order with respect to the polarization direction and mimic a prototypical polar glass. It is also obvious that B-site cations exhibit relatively more extensive fluctuations than the A-site cations in both poled and unpoled states. To obtain a quantitative measure of the extent of this ordering or disordering of the cations, an orientational order parameter S was calculated w.r.t. $[001]_{pc}$ for each cation as follows: $S = 1.5\langle cos^2\theta\rangle - 0.5$, where θ is the angle between $[001]_{pc}$ and $\delta\vec{r}$. Therefore, in general, the distributions of S-values can reveal specific ordering tendencies or disordering phenomena with respect to a chosen crystallographic direction (see also the Fig.2 caption). Figure2 shows the respective S-values for different cations in both states. As the stereographs remain qualitatively similar for all, i.e., there is no discrete change in the statistically favored preference of direction beyond the overall randomness around $[001]_{pc}$, the numbers in Fig.2 can be compared among the cations in both states. Hence, the changes in the S-values of the poled specimen suggest that the heavy A-site cations were greatly affected by the external field, leading to a larger reduction in their dispersions relative to lighter B-site cations. Apart from the obvious consequence on the emerging average structure of the system, this has important implications in identifying the local structural contributions to its macroscopic properties. For instance, the stereographs provide direct evidence that the system constitutes an ergodic polar state at this composition where both A and B-site cations exhibit alike local polarization correlation functions. Besides, the specific changes in the A-site cation displacements upon poling imply higher flexibility for them than the B-site cations, which further indicates that thermodynamically A-site cations experience a greater extent of strain-polarization decoupling in their local potential functions than the B-site cations. Hence, it can be expected that the electromechanical properties of the system at this composition would be determined by the more flexible A-site cations. This is probably a generic phenomenon in the case of $PbTiO_3$-based solid solutions, and in fact, one of the key factors that makes the disordered Pb-containing systems far better ferroelectric piezoelectric materials than the Pb-free systems in general. However, one should also bear in mind that parallel B-site substitutional disorder and heterovalency are also critical to facilitate the decoupling of off-axis A-site cation displacements from the lattice.

The mode values from the distributions of shift-magnitudes for different cations in poled and unpoled states are given in Fig.3, which shows that there is negligible changes in the polarity ($|\delta\vec{r}|$) and local polar heterogeneity ($\sigma(|\delta\vec{r}|)$) of the system upon poling. Notably, Bi shows maximum distortion among the cations, which is not surprising because Bi is usually found with a very distorted local environment in perovskite-based materials[35,36]. Considering the disorders observed in the stereographs and the distributions of magnitudes, it is clear that the reported structural modifications[23] (see also Fig. S1) on the application of an electric field is

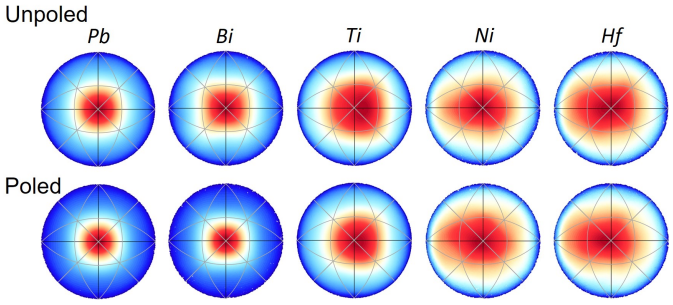


FIG. 1. $[001]_{pc}$ stereographs with the projected directions of the cation-displacements relative to their oxygen environments. Data from all 50 runs were combined to produce good statistics. The color of each point was assigned following the point-density around that point, thereby it helps to understand the trends of those directions along different crystallographic directions.

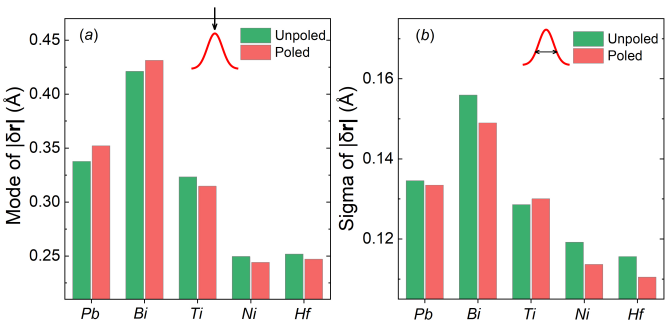


FIG. 3. Estimated values of (a) mode $|\delta\vec{r}|$ and their (b) standard deviations for different cations at poled and unpoled conditions.

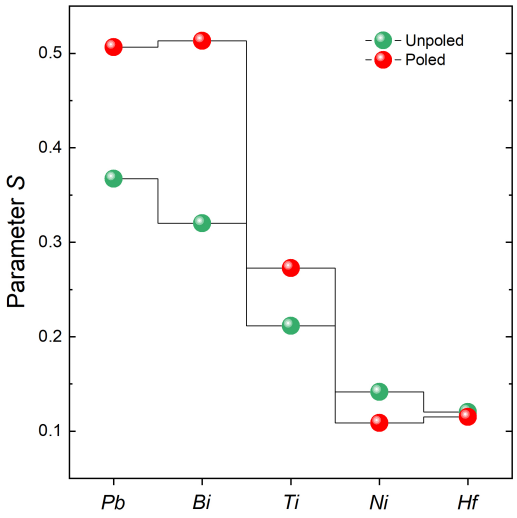


FIG. 2. Development of the orientation-order parameter S for different cations at poled and unpoled conditions. Parameter S should always be interpreted together with the stereographs presented in the paper. In the cases of similar distributions or trends, this parameter can serve as a quantitative description of the extent of order or disorder present within the system.

driven by the reconfigurable polar displacements, and simply a manifestation of length-scale dependent correlations. Individual cation-oxygen bond-length distributions obtained from the refined models are shown in Fig. S3 in SM[29] for all cations, which show no changes between the poled and unpoled samples, supporting the above inference.

To further understand the structure-property connection in this system, we have compared the present orientational disorders and mode values of $|\delta\vec{r}|$ of Pb and Ti cations against two other solid solutions at compositions where highest piezoelectric responses were found. It is apparent that xBNH-PT at $x = 0.39$ exhibits a very similar disordered state with reasonably large values of unit-cell polarizations compared to both xBi$(Ni_{0.5}Ti_{0.5})O_3$-PT and xBi$(Ni_{0.5}Zr_{0.5})O_3$-PT, which should be the key structural features responsible for its enhanced piezoelectricity. In addition, one can also envisage that in all three solid solutions, there is a high degree of structural homogeneity or ergodicity because A- and B-site cations exhibit alike isotropic distributions around [001], and it is well known that dipolar homogeneity or ergodicity promotes electric susceptibility[3,17]. Therefore, this comparative picture render strong evidence that the electromechanical properties are heavily dependent on the cation-specific disorder and their correlations or coupling to the polarization irrespective of the emerging macroscopic state or changes in the macroscopic structural models. In other words, the perturbations of the microscopic interaction parameter induced by different chemical species will ultimately determine the extents of intrinsic and various extrinsic factors that affect the piezoelectric properties significantly[24]. However, despite the much deeper understanding of the local structural correlations, the following question can still be raised : Why does xBNH-PT at $x = 0.39$ having equivalent dipolar disorder and relatively lower values of unit-cell polarization exhibit a bit higher piezoelectricity ($d_{33} \sim 440$ pC/N)[23] than either xBNT-PT ($d_{33} \sim 230$ pC/N) or xBNZ-PT ($d_{33} \sim 422$ pC/N) at $x = x_{MPB}$[37,38]?

To find potential answer to the above doubt, poled and unpoled ceramics of BNH-PT at $x = 0.39$ were further studied by Raman scattering at ambient conditions as well as at elevated temperatures. Although the spectral deconvolutions follow a similar pattern compared to other solid solutions reported recently[22,40], surprisingly, on this occasion, we have found a strong dependence of the Raman scattering intensity on the polarization of the incident light with respect to the scattered light in both poled and unpoled samples. Figure 5a shows the Raman spectra of poled and unpoled cearmics at two different setting: (1) Parallel polarized (pp), i.e. when the polarization of incident light is parallel to the polarization of scattered light, and (2) cross polarized (cp),

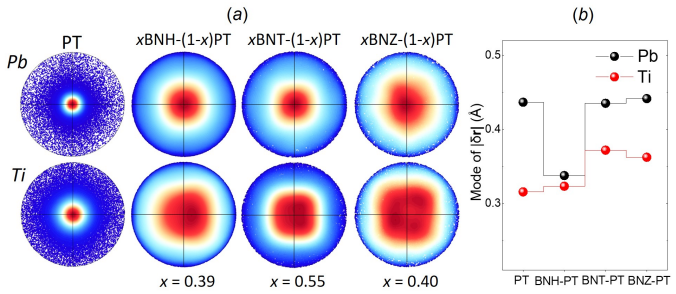


FIG. 4. (a) Stereographs of Pb and Ti displacement directions in three solid solutions with different B-site substitutions, plus unmodified $PbTiO_3$. (b) Corresponding mode $|\delta\vec{r}|$ values of the cations in those materials at the respective compositions[22,39].

meaning the polarization of incident light is perpendicular to the polarization of scattered light. Ideally, the Raman scattering from a single domain of a ferroelectric crystal should be polarized and orientation-dependent, and it should be unpolarized and orientation-independent for multi-domain polycrystalline samples. In our experiment, we have used a microscope with a 50x objective, for which the signal primarily comes from a semisphere with diameter ∼2 μm. Therefore, samples with crystallites of sizes in the range ∼20 – 100 nm should produce indistinguishable pp and cp spectra due to their random orientations within the probed volume. Consequently, the observation of polarization-dependent but orientation-independent spectral intensity for the polycrystalline sample having grain-sizes in the range 3 – 5 μm (Fig. S6[29]) is quite unusual and unanticipated. In fact, we did not detect any comparable feature in other analogues systems[21,22,40], nor did we find a reference where such an intensity dependence was recorded for a polycrystalline sample. Therefore, the well polarized spectra indicate that not only the correlation length of the coupled ferroic species are extremely small here, but also, the existence a highly polarizable matrix which causes the polarization-dependent intensity variations. Domain miniaturization is commonplace in ferroelectric solid solutions, which is also seen as a critical local structural feature causing high piezoelectricity in relaxor ferroelectrics and at the MPBs of complex solid solutions. However, in the current material, it is apparent that the chemical substitution, in particular, the addition of Hf has led to a responsive and polarizable matrix which is boosting the piezoelectric response of the system at a composition beyond MPB. It is also notable that the poling did not affect the extent and nature of the ferroic coupling because the depolarization ratio $I_{cp}/(I_{cp}+I_{pp})$ was comparable in both states of the sample. Moreover, when the sample was heated, the ratio remains constant until the system loses all its ferroic species at the high temperature paraelectric state well above the temperature T_m corresponding to the dielectric-permittivity peak shown in Fig. S5 (Fig.5c).

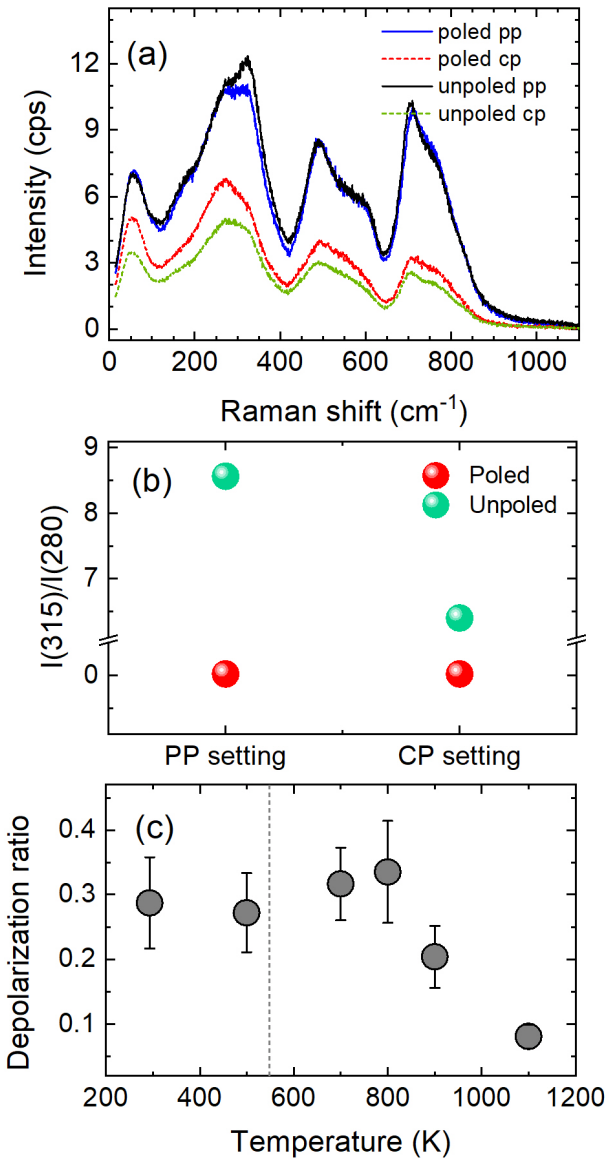


FIG. 5. (a) Normalized and temperature-reduced Raman spectra of xBNH-PT (x = 0.39) ceramics at pp and cp settings, as described in the text. The observations were substantiated by probing several areas on the smooth surface of a ceramic pellet. (b) Ratios of integrated intensities of the peaks at around 280 and 315 cm^{-1}. (c) Development of total depolarization ratio as a function of temperature in the case of unpoled ceramics. The dashed line marks the dielectric-maximum temperature T_m ∼ 548 K.

Nevertheless, the most pronounced poling-induced change found in the Raman spectra was an increase in the integrated intensity of the peak around 280 cm^{-1} relative to the peak around 315 cm-1, which is particularly significant in the PP setting (see Fig.5b). The Raman peak around 280 cm^{-1}corresponds to off-center displacements at the B site, whereas the 315 cm^{-1} peak arises from the antiphase tilting of the BO_6 octahedra[41–43], which are two local-scale competing orders (polar and antiferrodis-

tortive) related to the B-site sublattice in an ABO_3-type ferroelectric system. The antiphase tilting can also be accompanied by antipolar A-site cation displacements with components along the cubic body diagonals. Therefore, the reduction of $I_{pp}(315)/I_{pp}(280)$ ratio upon poling suggest the following mechanism promoting a field-induced local-scale as well as average tetragonal-type ordering as discussed earlier: The external electric field stimulates a local ordering at the B site, succeeding the tilt-driven antiferrodistortive order, which in turn affects the antipolar or non-collinear A-site-cation shifts and facilitates ordering at the A site. In fact, both A- and B-site ordering phenomena under electric field gracefully corroborates the development S parameters presented in Fig.2.

In summary, we have revealed interesting nano-scale structural correlations and dynamics that explain the anomalous structure-property behavior in xBNH-PT at $x = 0.39$. In particular, the combination of neutron total scattering and Raman scattering data analyses has helped to resolve the inherent structural distortion, defects, disorder, extent of correlations, coupling, dynamics, and potential mechanism behind the large piezoelectricity of xBNH-PT at a non-MPB composition. There is no doubt that xBNH-PT is a unique system where a responsive and polarizable matrix is amplifying its susceptibility to mechanical deformation beyond the typical structural instability factors. Notably, the results provide critical information for a non-trivial case in the context of understanding structure-property relationships for disordered and chemically-complex ferroelectric solid solutions, which is likely to play a important role in designing novel or improved electro-mechanical systems.

ACKNOWLEDGMENTS

Financial support from Deutsche Forschungsgemeinschaft is gratefully acknowledged. We are hugely grateful to David Keen (GEM, ISIS Facility, U.K.) for the assistance with the data collection and correction. K.D. would like to thank Matt Tucker (ORNL) for helpful discussions on the use of RMCProfile software. R. R. acknowledges the Science and Engineering Research Board (SERB) of the Ministry of Science and Technology, Govt. of India (Grant No.EMR/2016/001457) for financial assistance. A.U. is grateful to the Dr. D. S. Kothari Post-Doctoral Fellowship of UGC, India.

* kaustuv.datta@uni-hamburg.de

[1] T. Egami, Annu. Rev. Mater. Res. **37**, 297 (2007).
[2] A. Bussmann-Holder, H. Beige, and G. Völkel, Phys. Rev. B **79**, 184111 (2009).
[3] M. E. Lines and A. M. Glass, *Principles and Applications of Ferroelectrics and Related Materials* (Clarendon Press, Oxford, 1977).
[4] R. Blinc and B. Zeks, *Soft Modes in Ferroelectrics and Antiferroelectrics* (North-Holland, Amsterdam, 1974).
[5] Y. Yacoby and Y. Girshberg, AIP Conference Proceedings **535**, 56 (2000), https://aip.scitation.org/doi/pdf/10.1063/1.1324440.
[6] J. Frantti, Y. Fujioka, J. Zhang, S. C. Vogel, Y. Wang, Y. Zhao, and R. M. Nieminen, The Journal of Physical Chemistry B **113**, 7967 (2009), pMID: 19441804, http://dx.doi.org/10.1021/jp9024987.
[7] N. Zhang, H. Yokota, A. M. Glazer, Z. Ren, D. A. Keen, D. S. Keeble, P. a. Thomas, and Z.-G. Ye, Nat. Commun. **5**, 5231 (2014).
[8] O. Gindele, A. Kimmel, M. G. Cain, and D. Duffy, The Journal of Physical Chemistry C **119**, 17784 (2015), https://doi.org/10.1021/acs.jpcc.5b03207.
[9] N. Zhang, H. Yokota, A. M. Glazer, D. A. Keen, S. Gorfman, P. A. Thomas, W. Ren, and Z.-G. Ye, IUCrJ **5**, 73 (2018).
[10] K. M. Rabe, Nature Materials **1**, 147 (2002).
[11] I. Grinberg, V. Cooper, and A. Rappe, Nature **419**, 909 (2002).
[12] D. A. Keen, IUCrJ **3**, 8 (2016).
[13] A. L. Goodwin, Nature Communications **10**, 10 (2019).
[14] M. J. Krogstad, P. M. Gehring, S. Rosenkranz, R. Osborn, F. Ye, Y. Liu, J. P. Ruff, W. Chen, J. M. Wozniak, H. Luo, O. Chmaissem, Z. G. Ye, and D. Phelan, Nature Materials **17**, 718 (2018).
[15] M. Eremenko, V. Krayzman, A. Bosak, H. Y. Playford, K. W. Chapman, J. C. Woicik, B. Ravel, and I. Levin, Nature Communications **10**, 2728 (2019).
[16] V. Petkov, J.-W. Kim, S. Shastri, S. Gupta, and S. Priya, Phys. Rev. Materials **4**, 014405 (2020).
[17] K. Datta, K. Brajesh, R. Ranjan, and B. Mihailova, Phys. Rev. B **060102(R)**, 1 (2020).
[18] R. Eitel, C. Randall, T. Shrout, P. Rehrig, W. Hackenberger, and S.-E. Park, Jpn. J. Appl. Phys. **40**, 5999 (2001).
[19] I. Grinberg, M. R. Suchomel, P. K. Davies, and A. M. Rappe, Journal of Applied Physics **98**, 094111 (2005), https://doi.org/10.1063/1.2128049.
[20] K. Uchino, Science and Technology of Advanced Materials **16**, 046001 (2015), https://doi.org/10.1088/1468-6996/16/4/046001.
[21] K. Datta, R. B. Neder, J. Chen, J. C. Neuefeind, and B. Mihailova, Scientific Reports **7**, 471 (2017).
[22] K. Datta, R. B. Neder, J. Chen, J. C. Neuefeind, and B. Mihailova, Phys. Rev. Lett. **119**, 207604 (2017).
[23] U. Shankar, N. Kumar, B. Narayan, D. Swain, A. Senyshyn, and R. Ranjan, Phys. Rev. B **100**, 094101 (2019).
[24] D. Damjanovic, J. Amer. Ceram. Soc. **88**, 2663 (2005).
[25] D. Damjanovic, Applied Physics Letters **97**, 062906 (2010), https://doi.org/10.1063/1.3479479.
[26] P. Day, J. Enderby, W. Williams, L. Chapon, A. Hannon, P. Radaelli, and A. Soper, Neutron News **15**, 19 (2004), https://doi.org/10.1080/00323910490970564.
[27] M. G. Tucker, D. A. Keen, M. T. Dove, A. L. Goodwin, and Q. Hui, J. Phys.: Condens. Matter **19**, 335218 (2007).
[28] R. B. Neder and T. Proffen, *Diffuse scattering and defect*

structure simulations - A cook book using the program DISCUS (Oxford University Press, UK, 2007).

[29] See Supplemental Material [url] for additional figures and more details on the data analyses. It also contains the References 26, 29 and 41.

[30] T.Egami and S. Billinge, *Underneath the Bragg Peaks Structural Analysis of Complex Materials* (Pergamon Materials Series, 2012).

[31] D. A. Keen, J. Appl. Cryst. **34**, 172 (2001).

[32] H. Y. Playford, L. R. Owen, I. Levin, and M. G. Tucker, Annual Review of Materials Research **44**, 429 (2014), https://doi.org/10.1146/annurev-matsci-071312-121712.

[33] D. A. Keen, Crystallography Reviews **26**, 143 (2020), https://doi.org/10.1080/0889311X.2020.1797708.

[34] R. Resta, Rev. Mod. Phys. **66**, 899 (1994).

[35] D. S. Keeble, E. R. Barney, D. A. Keen, M. G. Tucker, J. Kreisel, and P. A. Thomas, Adv. Funct. Mater. **23**, 185 (2013).

[36] K. B. Tio, I. Levin, D. S. Keeble, G. Cibin, H. Y. Playford, M. Eremenko, V. Krayzman, W. J. Laws, and I. M. Reaney, Chemistry of Materials **31**, 2450 (2019).

[37] Q. Zhang, M. Jiang, and Z. Li, Journal of Electroceramics **29**, 179 (2012).

[38] Y. Rong, J. Chen, H. Kang, L. Liu, L. Fang, L. Fan, Z. Pan, and X. Xing, Journal of the American Ceramic Society **96**, 1035 (2013), https://ceramics.onlinelibrary.wiley.com/doi/pdf/10.1111/jace.12236.

[39] K. Datta, I. Margaritescu, D. A. Keen, and B. Mihailova, Physical Review Letters **121**, 137602 (2018).

[40] I. Margaritescu, K. Datta, J. Chen, and B. Mihailova, Journal of Raman Spectroscopy **51**, 1200 (2020), https://analyticalsciencejournals.onlinelibrary.wiley.com/doi/pdf/10.1

[41] A.-M. Welsch, B. J. Maier, B. Mihailova, R. J. Angel, J. Zhao, C. Paulmann, J. M. Engel, M. Gospodinov, V. Marinova, and U. Bismayer, Z. Kristallogr. **226**, 126 (2011).

[42] B. J. Maier, A.-M. Welsch, B. Mihailova, R. J. Angel, J. Zhao, C. Paulmann, J. M. Engel, W. G. Marshall, M. Gospodinov, D. Petrova, and U. Bismayer, Phys. Rev. B **83**, 134106 (2011).

[43] G. de la Flor, T. Malcherek, S. Gorfman, and B. Mihailova, Phys. Rev. B **96**, 214102 (2017).